

RESEARCH ARTICLE

10.1002/2017MS001009

Multilocalization data assimilation for predicting heavy precipitation associated with a multiscale weather system

Shu-Chih Yang^{1,2}, Shu-Hua Chen³ , Keichii Kondo² , Takemasa Miyoshi² , Yu-Chiang Liou^{1,4} , Yung-Lin Teng¹, and Hui-Ling Chang⁵

Key Points:

- Improving large-scale moisture transport and small-scale convergence are critical to Meiyu rainfall forecasts
- A multiscale weather system needs multiscale corrections in high-resolution EnKF analysis
- EnKF with dual localizations improves the intensity and time variation of the short-lasting, intense heavy rainfall prediction

Correspondence to:

S.-H. Chen,
shachen@ucdavis.edu

Citation:

Yang, S.-C., S.-H. Chen, K. Kondo, T. Miyoshi, Y.-C. Liou, Y.-L. Teng, and H.-L. Chang (2017), Multilocalization data assimilation for predicting heavy precipitation associated with a multiscale weather system, *J. Adv. Model. Earth Syst.*, 9, 1684–1702, doi:10.1002/2017MS001009.

Received 6 APR 2017

Accepted 17 JUN 2017

Accepted article online 20 JUN 2017

Published online 13 JUL 2017

© 2017. The Authors.

This is an open access article under the terms of the Creative Commons Attribution-NonCommercial-NoDerivs License, which permits use and distribution in any medium, provided the original work is properly cited, the use is non-commercial and no modifications or adaptations are made.

¹Department of Atmospheric Sciences, National Central University, Taoyuan, Taiwan, ²RIKEN Advanced Institute for Computational Science, Kobe, Japan, ³Department of Land, Air and Water Resources, University of California, Davis, California, USA, ⁴Taiwan Typhoon and Flood Research Institute, Taipei, Taiwan, ⁵Research and Development Center, Central Weather Bureau, Taipei, Taiwan

Abstract High-resolution numerical simulations are regularly used for severe weather forecasts. To improve model initial conditions, a single short localization is commonly applied in the ensemble Kalman filter when assimilating observations. This approach prevents large-scale corrections from appearing in a high-resolution analysis. To improve heavy rainfall forecasts associated with a multiscale weather system, analyses must be accurate across a range of spatial scales, a task that is difficult to accomplish using a single localization. This study is the first to apply a dual-localization (DL) method to improve high-resolution analyses used to forecast a real-case heavy rainfall event associated with a Meiyu front on 16 June 2008 in Taiwan. A Meiyu front is a multiscale weather system characterized by storm-scale convection, a mesoscale front, and large-scale southwesterly monsoonal flow. The use of the DL method to produce the analyses was able to correct both the synoptic-scale moisture flux transported by southwesterly monsoonal flow and the mesoscale low-level convergence offshore of southwestern Taiwan. As a result, the forecasted amount, pattern, and temporal evolution of the heavy rainfall event were improved.

1. Introduction

Heavy rainfall forecasts receive great attention from society because of their significant impact on human lives and Property. Due to improved computing capabilities, weather prediction is now commonly carried out using a high-resolution regional numerical model with a horizontal grid spacing of just a few km, particularly for severe weather systems that include convective clouds. Coupling data assimilation with a high-resolution numerical model can greatly improve severe weather prediction by correcting storm-scale errors where observation density is high [Sun *et al.*, 2014]. For example, the high-resolution Ensemble Kalman Filter (EnKF) has been used to assimilate high-frequency, high-density radar data to aid storm-scale prediction [Zhang *et al.*, 2004, 2009; Zhao *et al.*, 2013; Tsai *et al.*, 2014]. To further improve forecast skill particularly for longer forecast times, however, the large-scale environment upstream of a severe weather system should also be represented as accurately as possible in the initial conditions. This is especially important for weather systems characterized by multiscale interactions, such as tropical cyclones and frontal systems. In such situations, it would be preferable to design and use a unified data assimilation framework to perform multiscale, multiresolution assimilation to improve high-resolution weather forecasts.

In EnKF, the flow-dependent background error covariance structures determine how observation information is spread out to form the analysis increments. Since the number of ensemble members used is necessarily finite, sampling errors can result in spurious background error correlations, leading to false analysis corrections [Miyoshi *et al.*, 2014; Poterjoy *et al.*, 2014] particularly for large-wave number (i.e., small-scale) components of grid-resolved atmospheric motions [Raynaud *et al.*, 2009]. This issue can be avoided by applying the covariance localization method [Houtekamer and Mitchell, 1998; Hunt *et al.*, 2007; Greybush *et al.*, 2012], which limits the observation influence to within a certain localization radius. The choice of the localization distance should depend on the characteristic scale of the atmospheric instabilities of interest and the observation density. A typical horizontal localization distance is on the order of 1000 km for synoptic-scale instabilities [Whitaker *et al.*, 2008], 100 km for mesoscale, and few kilometers for storm-scale instabilities [Zhang *et al.*, 2006].

Several studies have tried to determine how to best implement multiscale corrections. *Zhang et al.* [2009] proposed a successive covariance localization method, in which they selected radar observation subsets of differing densities for different nested model domains to correct errors across a range of spatial scales, including synoptic scale, mesoscale, and storm scale for both coarse- and fine-resolution domains, respectively. For a different application, *Miyoshi and Kondo* [2013] and *Kondo et al.* [2013] proposed a dual-localization (DL) method to combine EnKF analysis corrections for different spatial scales in the same domain. The analysis corrections for different scales of atmospheric motions were derived separately from the full-resolution and small-wave number components (i.e., large-scale systems) of the background ensemble perturbations before being combined. Recently, *Li et al.* [2015] reformulated the cost-function used in oceanic variational analysis by decomposing the background error covariance into large and small-scale components and computing the cross-covariance between large and small-scale errors, ultimately producing analysis corrections appropriate for multiple spatial scales and grid resolutions. We note that a high observation density is required for the methods outlined in *Zhang et al.* [2009] and *Li et al.* [2015], but not for the DL method. The observations used in this study, which are used to improve the forecast of a multiscale Meiyu front over Southeast Asia, are sparse at certain times and over particular areas, making the DL method the most appropriate option.

Meiyu fronts (called Baiu fronts in Japan and Jangma in Korea), which cause episodes of heavy precipitation during the Meiyu season, are typical examples of multiscale weather systems. Meiyu fronts are stationary fronts that occur over Southeast Asia from late spring through early summer. Rainfall from Meiyu fronts represents a critical source of water for eastern China, Taiwan, Korea, Japan, and even eastern Russia, but can sometimes also cause severe mudslides and flooding. Thus, accurately forecasting the onset, amounts, and distribution of Meiyu rainfall and understanding the mechanisms that control it are important challenges from both scientific and societal points of view. However, both of these issues can be complicated by the fact that a Meiyu front is a multiscale weather system involving storm-scale convective clouds, a mesoscale front and potentially one or more mesoscale convective systems, and large-scale southwesterly monsoonal flow. Additional complexity can arise from interactions with complex terrain. Field experiments, such as the Southwest Monsoon Experiment (SoWMEX) and the Terrain-Influenced Monsoon Rainfall Experiment (TiMREX) [*Jou et al.*, 2011], have been conducted to improve Meiyu rainfall forecasts and our understanding of the multiscale physical and dynamical processes involved in them.

Yang et al. [2014, hereafter Y2014] used a regional EnKF system to predict a heavy precipitation episode on 16 June 2008 during SoWMEX/TiMREX. Using a flow-dependent background error covariance, they showed that the moisture analysis can be significantly improved by assimilating observations, particularly COSMIC (Constellation Observing System for Meteorology, Ionosphere, and Climate) Global Positioning System Radio Occultation (GPS-RO) local bending angles, leading to a skillful prediction of accumulated rainfall in southwestern Taiwan. However, the predicted evolution of short-term rainfall intensities did not agree well with observations, which in an operational forecast setting could lead to poor anticipation of the flash flood threat, potentially endangering human lives. To better represent convective-scale features, this study seeks to apply data assimilation to a high-resolution model grid for the same heavy rainfall case examined in Y2014. However, given the multiscale nature of a Meiyu front, optimal analysis corrections should minimize errors at different scales that may affect the development of the severe weather system. This includes synoptic-scale moisture transport (i.e., monsoonal flow), the mesoscale stationary front and mesoscale convective systems, convective clouds, and local geographical effects (i.e., land-sea contrast and complex terrain). These are factors that affect the moisture flux and the location and amplitude of convergence and vertical motion. To improve heavy rainfall forecasts for multiscale Meiyu frontal systems, we introduce a multiresolution, multiscale assimilation framework that applies the DL method to the inner domain analysis of a nested-domain model configuration. The success of this approach is evaluated using the heavy precipitation event on 16 June 2008, the same case studied in Y2014. Our study marks the first time that the DL method has been applied to a high-resolution mesoscale model using real observations for a heavy precipitation event. This is a leap forward from *Miyoshi and Kondo* [2013], who developed the DL method and showed its potential with an observation simulation system experiment (OSSE) that used a simplified atmospheric general circulation model. A mesoscale model usually uses high-resolution grids to resolve small-scale to mesoscale weather systems. Therefore, analyses produced using multiscale error corrections could greatly improve forecasts of multiscale severe weather events, the primary focus of this study.

The paper is organized as follows: section 2 presents the multiresolution, multiscale assimilation framework and experimental setup. Results from the analyses and forecasts are presented and discussed in sections 3 and 4, respectively. Finally, concluding remarks are given in section 5.

2. Method

2.1. Multiresolution and Multiscale Localization Data Assimilation Framework

As mentioned section 1, although a short localization is usually used for high-resolution analyses due to sampling error considerations, it may not always prove optimal for multiscale weather forecasts. To tackle this multiscale analysis issue, a dual-resolution, dual-localization (DL) data assimilation framework is established based on the regional analysis system developed by *Yang et al.* [2013] and the DL method developed by *Miyoshi and Kondo* [2013]. The regional analysis system, developed at the National Central University (NCU) in Taiwan, couples the Local Ensemble Transform Kalman Filter [*Hunt et al.*, 2007] with the Weather Research and Forecasting model [*Skamarock and Klemp*, 2008] (WRF-LETKF). The LETKF algorithm belongs to a group of EnKF algorithms known as deterministic EnKFs [*Houtekamer and Zhang*, 2016]. It updates both the background (short-range forecast) ensemble mean and perturbations from the mean. The LETKF analysis corrections are based on the background ensemble perturbations. During data assimilation cycling, the WRF model is used to produce the short-range nested-domain forecasts, where the coarse-resolution domain is used to resolve synoptic-scale to mesoscale systems while the high-resolution domain is used to resolve finer-scale atmospheric features. For the coarse-resolution outer domain, we applied LETKF data assimilation with a single, long-distance horizontal localization. For the finer-resolution inner domain, we applied data assimilation using both long- and short-distance localizations (i.e., the DL method). Below, the DL method is briefly introduced. Readers wanting additional information about the DL method are referred to *Miyoshi and Kondo* [2013].

Equation (1) reveals the components involved in the DL method. In equation (1), \mathbf{x}^a and \mathbf{x}^b are the analysis and background states, respectively, and $(\mathbf{x}^a - \mathbf{x}^b)$ represents the analysis corrections.

$$(\mathbf{x}^a - \mathbf{x}^b)_{DL} = (\mathbf{x}^a - \mathbf{x}^b)_{SLoc}^{full} + \left[(\mathbf{x}^a - \mathbf{x}^b)_{LLoc}^{swc} - (\mathbf{x}^a - \mathbf{x}^b)_{SLoc}^{swc} \right] \quad (1)$$

When using the DL method for high-resolution data assimilation, the analysis corrections within and beyond the range of the short localization are derived from the original, full-resolution background ensemble perturbations (*full*) and its small-wave number components (*swc*), respectively. These analysis corrections are then merged to form the high-resolution, multiscale analysis. Below is the detailed procedure for using the dual-localization LETKF:

1. Derive the analysis correction with a short localization (*SLoc*) from the original, full-resolution ensemble perturbations (*full*). The result is the first term on the right-hand (RHS) side of equation (1)
2. Derive the large-scale, analysis correction with a long localization (*LLoc*) from the small-wave number components (*swc*) of the ensemble perturbations, which are obtained by applying a low-pass Lanczos filter to said perturbations. The critical wavelength of the Lanczos filter is set to $10 \Delta x$ (90 km for this high-resolution ensemble perturbation). The result of this step corresponds to the second term on the RHS of equation (1).
3. Derive the large-scale, analysis correction with a *SLoc* from the small-wave number components (*swc*) of the ensemble perturbations, obtained and used in step (2). The result corresponds to the last term on the RHS of equation (1). The large-scale correction beyond the short localization range, represented by the bracketed term in equation (1), is then obtained by subtracting the correction obtained in this step from that obtained in step (2). The subtraction is necessary to avoid "double-counting" the large-scale correction within the short localization range.
4. Merge the results of steps 1 and 3 to finalize the multiscale corrections and then add them to the background ensemble to produce the analysis ensemble.

2.2. Experimental Setup

This multiresolution, dual-localization data assimilation system is evaluated using the heavy precipitation event that occurred on 16 June 2008 during SoWMEX/TiMREX [*Davis and Lee*, 2012; *Xu et al.*, 2012]. The heavy rainfall was caused by strong mesoscale convective systems embedded in general southwesterly

monsoonal flow that developed offshore of southwestern Taiwan before moving inland. The strong southwesterly flow over the northeastern South China Sea advected abundant moisture toward southwestern Taiwan, where it turned southerly due to Taiwan's topography and surface friction, which resulted in low-level convergence over Taiwan's southwestern coast. These conditions aided the development of heavy precipitation systems over the region [Xu *et al.*, 2012]. Low-level convergence was further enhanced by cold pool outflow caused by rainfall evaporation over southwestern Taiwan on 14–15 June. Such a period of sustained convergence led to an extended period of heavy precipitation on 16 June [Tu *et al.*, 2017].

Y2014 used the WRF-LETKF with one domain (27 km resolution) and a single localization to study the same Meiyu event. This study extends the work of Y2014 by using the DL method to assess the impact of high-resolution, multiscale analysis corrections on extreme precipitation forecasts. We are particularly interested in determining the benefit of assimilating observations from 15 June with nested domains on heavy rainfall forecasts for the following day. The focus on observations on 15 June aims to highlight the impact of the DL method under high-resolution assimilation framework while adopting the advantage of the synoptic-scale pattern that has been discussed in Y2014.

Three numerical experiments, in which high-resolution analyses are created with different localization strategies and used to produce forecasts for the heavy rainfall event, are conducted. For all experiments, the background ensemble is obtained from the 6 h ensemble forecasts (rather than perturbed global reanalysis data), which were initialized by the BANGLE analysis ensemble at 1800 UTC, 14 June 2014 produced by Y2014. Assimilation cycles were then performed at 6 h intervals through 1800 UTC, 15 June for all three experiments.

The BANGLE analysis ensemble from Y2014 was created by assimilating conventional meteorological observations, satellite wind vectors, and COSMIC RO bending angles on a single domain with a horizontal resolution of 27 km and 27 vertical levels. Data assimilation was performed between 0000 UTC 13 June and 1800 UTC 15 June 2008 at 6 h intervals using 36 ensemble members whose initial conditions were centered on the National Centers for Environmental Prediction's (NCEP) Global Forecast System (GFS) Final Analysis (FNL) data. The single localization scale, defined as the Gaussian 1 sigma distance in the R-localization scheme [Hunt *et al.*, 2007], in Y2014 was 360 km. Y2014 demonstrated that the large-scale features in the BANGLE analysis on 15 June are important for accurately predicting the heavy rainfall on 16 June in southwestern Taiwan. There are two reasons why we used the 6 h ensemble forecasts at 0000 UTC 15 June from BANGLE as our initial background ensemble. First, it reduces the spin-up time of the ensemble perturbations associated with mesoscale dynamical instabilities [Pu *et al.*, 2016]. Second, and more importantly, the use of BANGLE forecasts to initialize each experiment's analysis-cycling period at 0000 UTC 15 June allows us to more confidently ascribe differences in subsequent heavy rainfall forecasts to the use of different high-resolution data assimilation strategies. Note that the initial time of the analysis-cycling period was chosen so that observations taken on 15 June, which are critically important to the success of the rainfall forecast, would be assimilated.

From 0000 UTC 15 June onward, the three experiments conducted in this study assimilate the same observations as used in BANGLE but for two domains rather than one (27 and 9 km resolution for the outer and inner domains, respectively). The experiments differ only in the localization strategy used for assimilation in the inner-domain (domain 2), which are a single-short (60 km), single-long (360 km), and dual-distance (360 and 60 km) localization. These experiments will be referred to as D02SS, D02SL, and D02DL, respectively. Only a single localization (360 km) is used for domain 1. Note that 60 and 360 km single-localizations allow error corrections to extend to about 180 and 1000 km from an observation location, respectively. These localization lengths were chosen to represent the characteristic scales of both synoptic-scale moisture transport (about 1000 km) and local mesoscale convective characteristics (100 km), including topographic effects, that characterized the heavy rainfall event in question. An 8% multiplicative covariance inflation was used to help compensate for underestimated background error covariances. As mentioned earlier, four assimilation cycles were performed between 0000 and 1800 UTC, 15 June for all three experiments. Figure 1 shows the spatial coverage of the observation types used for assimilation on 1200 UTC, 15 June. As will be discussed in section 3, the sounding data over the South China Sea play an important role in improving the moisture transport from that region to Taiwan.

One forecast, initialized by the analyses at 1200 UTC, 15 June, was conducted for each experiment. Each forecast was run with an additional high-resolution (3 km) nested domain (Figure 1) to better resolve

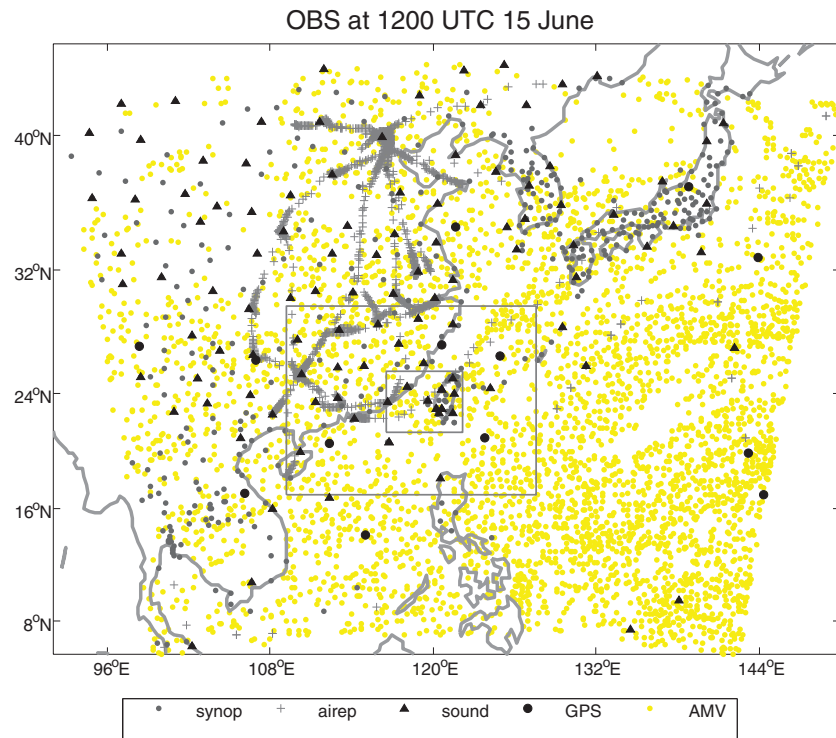


Figure 1. The types and location of the observations used for assimilation. The grey boxes from the largest to the smallest are domains 1–3, respectively.

convective clouds. The physics parameterizations used in all simulations were the Rapid Radiative Transfer Model (RRTM) longwave radiation scheme [Mlawer *et al.*, 1997], the Dudhia [1989] shortwave radiation scheme, the Yonsei University (YSU) PBL scheme [Hong *et al.*, 2006], the Grell-Devenyi ensemble cumulus scheme [Grell and Dévényi, 2002], and the Goddard cumulus ensemble (GCE) microphysics scheme [Tao *et al.*, 2003]. Note that no cumulus scheme was used in domain 3 due to its high spatial resolution. Forecasts were run out to 1600 UTC, 16 June to evaluate their rainfall predictions on 16 June (local date/time). The time step used for domain 1 was 90 s.

3. Results of Analysis

In this section, we examine and compare the domain-2 analysis corrections from each of the experiments. The examination focuses on features of the analyses relevant to the development and maintenance of the heavy rainfall event, such as those linked to large-scale moisture transport and small-scale convergence. Note that since the resolution of the background ensemble (6 h forecasts) for domain 2 is 9 km, one should only interpret model features larger than 54 km (the effective resolution of the dynamical core [Skamarock, 2004]). Thus, our discussion of the mesoscale elements of the analyses focuses on those whose sizes range from about 50 to 180 km (3 times the short localization distance). Note that in the following the mesoscale features are referred to small scales, in contrast to the large-scale features.

3.1. Impact on Large-Scale Moisture Transport

Figure 2 shows the wind and moisture analyses at 1200 UTC and 1800 UTC, 15 June, while Figure 3 shows the corresponding analysis increments at 1200 UTC, 15 June to illustrate the corrections made by different assimilation strategies. First, all three experiments show similar wind patterns at 1200 UTC, 15 June (Figures 2a–2c), which may be due to an abundance of satellite air-motion vector (AMV) data. Nevertheless, significant differences between the analyses are also present. Two such differences stand out. One is the much higher moisture content of the analyses created with a long localization (D02DL and D02SL) relative to that produced with just a single short localization (D02SS), particularly over an area extending from the South

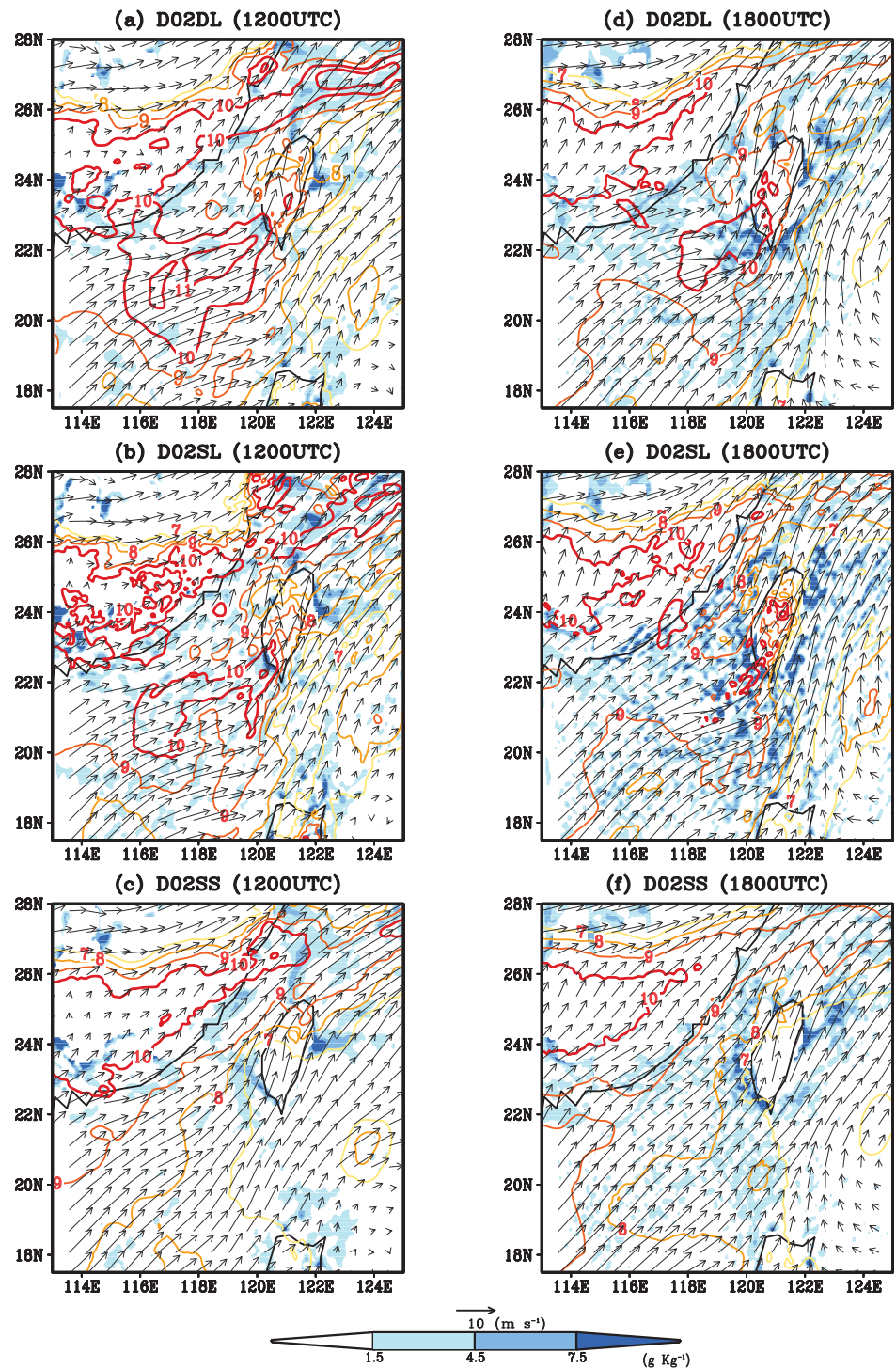


Figure 2. (a) Water vapor mixing ratio (g kg^{-1} , color contour) and wind vector analyses at 700 hPa and convergence ($\times 10^{-4} \text{ s}^{-1}$, color shading) at 975 hPa from D02DL at 1200 UTC 15 June 2008. Figures 2b and 2c are the same as Figure 2a, except from D02SL and D02SS, respectively. Figures 2d–2f are the same as Figures 2a–2c, respectively, except at 1800 UTC 15 June.

China Sea to Taiwan’s southwestern coast. At this time (i.e., 1200 UTC, 15 June), D02DL and D02SL both show a large-scale moisture correction embedded within southwesterly monsoonal flow, extending from the South China Sea to the southwestern coast of Taiwan (Figures 3a and 3b). No such moisture correction

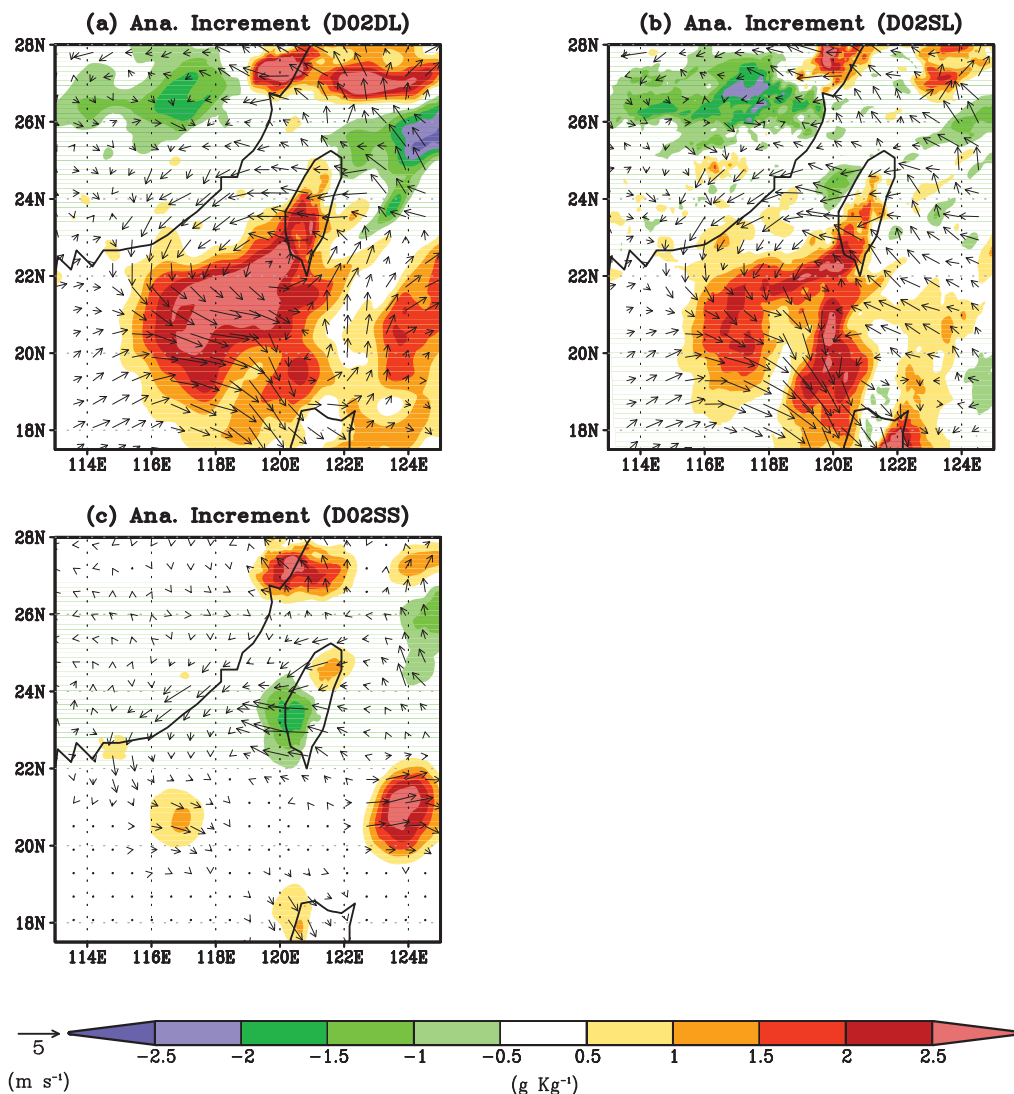


Figure 3. Water vapor mixing ratio (g kg^{-1}) and wind vector analysis increments at 700 hPa for (a) D02DL, (b) D02SL, and (c) D02SS at 1200 UTC 15 June, 2008.

exists for D02SS. Instead, Figure 3c shows that its analysis corrections are limited to areas near the observation locations. Note that although large-scale corrections are applied in both D02DL and D02SL, their magnitudes and patterns can be still quite different, as is the case for the large-scale moisture corrections over the South China Sea (Figure 3a versus Figure 3b).

The second notable difference between the analyses is that unlike the analyses of D02DL and D02SS, that from D02SL contains numerous small-scale convergence features (Figures 2b and 2e). These arise through the flow-dependent background error covariance and can appear long distances from their observation locations due to the use of a single long localization on a high-resolution model grid. Such widespread, small-scale correlations, however, may not be realistic and could interact with large-scale patterns and trigger false convection.

The wind analysis increments of both D02DL and D02SL (Figures 3a and 3b) consistently show mesoscale cyclonic patterns that enhance the development of the mesoscale convective system offshore of southwestern Taiwan [Xu et al., 2012; Tu et al., 2014]. The stronger westerly wind component over the South China Sea in these experiments helps increase moisture transport toward Taiwan. Those of D02SS, on the other hand, show a weaker and less coherent cyclonic pattern (Figure 3c), which causes the moisture

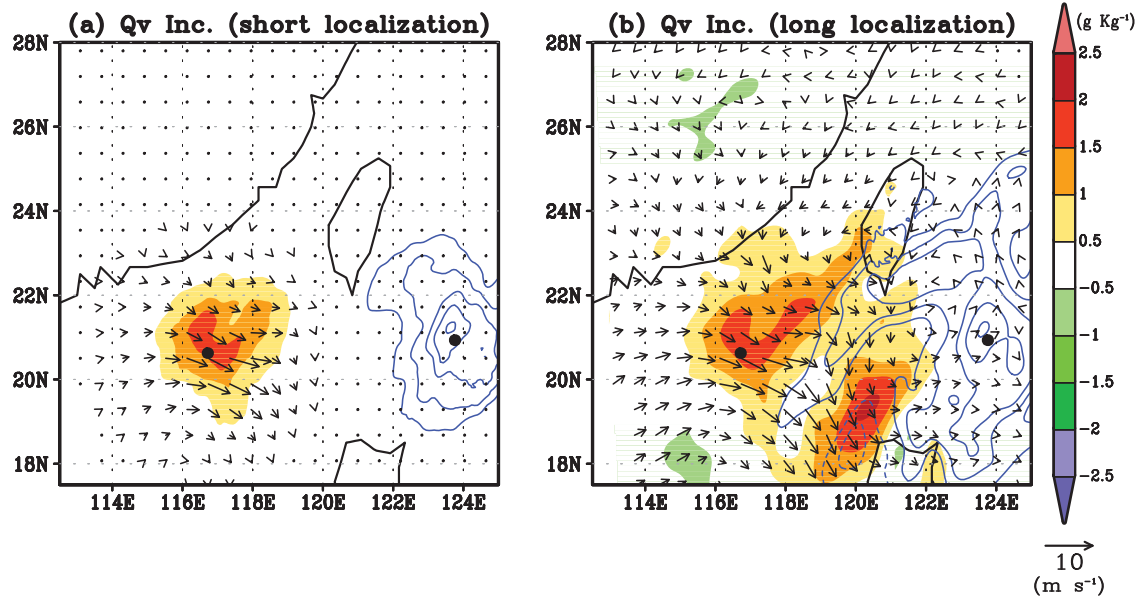


Figure 4. Water vapor mixing ratio (g kg^{-1}) and wind vector analysis increments at 700 hPa from the assimilation of a radiosonde (116.72°E , 20.67°N ; shading) and a GPS-RO sounding (123.76°E , 20.98°N ; blue contours) at 1200 UTC 15 June 2008 using (a) a single short localization and (b) a single long localization with the filtered ensemble perturbations (step 2 of the DL method, section 2.1). Two observation locations are indicated by black dots.

transport toward southwestern Taiwan to be insufficient to support the observed heavy rainfall event. The radiosonde observation at Pin-Dong in southern Taiwan plays a significant role in creating this negative moisture correction. D02SL and D02DL are not nearly as affected by this radiosonde observation due to the use of a long localization, which extends the range of influence of nearby observations and reduces the influence of the radiosonde observation on the analysis increments in this area.

Further analysis indicates that two observations are critical for remotely producing the pattern of the analysis corrections shown in Figures 3a and 3b. One is the radiosonde at Dongsha Island (116.72°E , 20.67°N) and the other is the GPS RO northeast of the Philippines (123.76°E , 20.98°N). When a short localization is applied to the high-resolution inner domain, the observation impact is limited to the observation locations and their immediate surroundings, capturing some small-scale features (Figure 4a). Conversely, when a long localization is applied, the observation impact spreads across a much larger area (Figure 4b) through the flow-dependent background error covariance. We note that Figure 4b is derived during the second step of the DL method, described in section 2.1, which generates a long-localization analysis using the small-wave number components of the ensemble perturbations. Note that in the second step the large-wave number components of ensemble perturbations were filtered out before producing the long-localization analysis. This is done to avoid introducing noisy, small-scale corrections to synoptic-scale features. As a result, the assimilation of these two observations increases atmospheric moisture over a wide area offshore of southwestern and southeastern Taiwan. As will be shown in the next section, the resulting large-scale moisture transport eventually leads to strong convection and heavy precipitation in D02DL and D02SL. The D02SS forecast proves to be the driest of the three experiments primarily due to inadequate moisture transport toward southwestern Taiwan in the analyses, caused by the use of a short localization.

3.2. Impact on Small-Scale Corrections

In addition to upstream large-scale wind and moisture advection, small-scale analysis features in southwestern Taiwan also play an important role in forecasting the development of the mesoscale convective system. As shown in Figure 2, low-level convergence in the analyses of all three experiments have similar small-scale structures and strong amplitudes over the frontal region near 119°E and 25.5°N at 1200 UTC, 15 June and the region offshore of southwestern Taiwan. A closer examination reveals that the convergence zone offshore of southwestern Taiwan covers a larger area in the D02DL analysis at 1800 UTC, 15 June than that in the D02SS analysis (Figure 2d versus Figure 2f), but is most extensive in the D02SL analysis, which also

has the largest convergence values in this region among the three experiments. This can lead to differences between the experiments' vertical velocity fields. It is important to note that while the analyses for all experiments show strong convergence offshore and along the coast of southwestern Taiwan, the D02SS analysis is much drier than the other two and lacks the large-scale conditions necessary to support persistent strong convection over Taiwan.

The impact of small-scale analysis corrections in the experiments are further examined by comparing the 700 hPa vertical velocity of the analyses to observations in and near southwestern Taiwan (Figure 5). The analyses at 1800 UTC, 15 June are examined since strong convection offshore of southwestern Taiwan had begun to develop at that time. The observed vertical velocity is derived from radar wind observations taken from the Wind Synthesis System using Doppler Measurement (WISSDOM) [Liou et al., 2014]. WISSDOM is obtained by applying a variational method [Liou et al., 2012] to data from S-band radar systems at Chigu and Kent-Ting, operated by Taiwan Central Weather Bureau (CWB), and S-POL deployed by the National Center for Atmospheric Research (NCAR). Since WISSDOM has a much higher spatial resolution (1 km) than the model analysis, waves shorter than 54 km (the effective resolution of the dynamical core in domain 2) are filtered out of the data to facilitate comparison with the analyses. All three analyses in Figure 5 show upward motion offshore of southwestern Taiwan, extending to the coast, associated with the developing mesocale vortex, but the updraft centered just offshore of the Kaoshiung county coastline (120°E, 22.4°N) is much stronger in the D02DL and D02SL analyses (Figures 5a and 5b) compared to that in the D02SS analysis (Figure 5c). However, this offshore updraft is larger and its maximum is shifted southward in the D02SL analysis. This updraft plays a particularly important role in the formation of strong convection that eventually makes its way onshore, producing heavy rainfall [Xu et al., 2012].

To further explain the differences between Figures 5a and 5b, we examine the vertical velocity corrections obtained by assimilating horizontal winds from a single radiosonde at Dongsha Island (marked with a black dot in Figures 6a–6c) at 1200 UTC, 15 June using the full-resolution perturbations and different localization

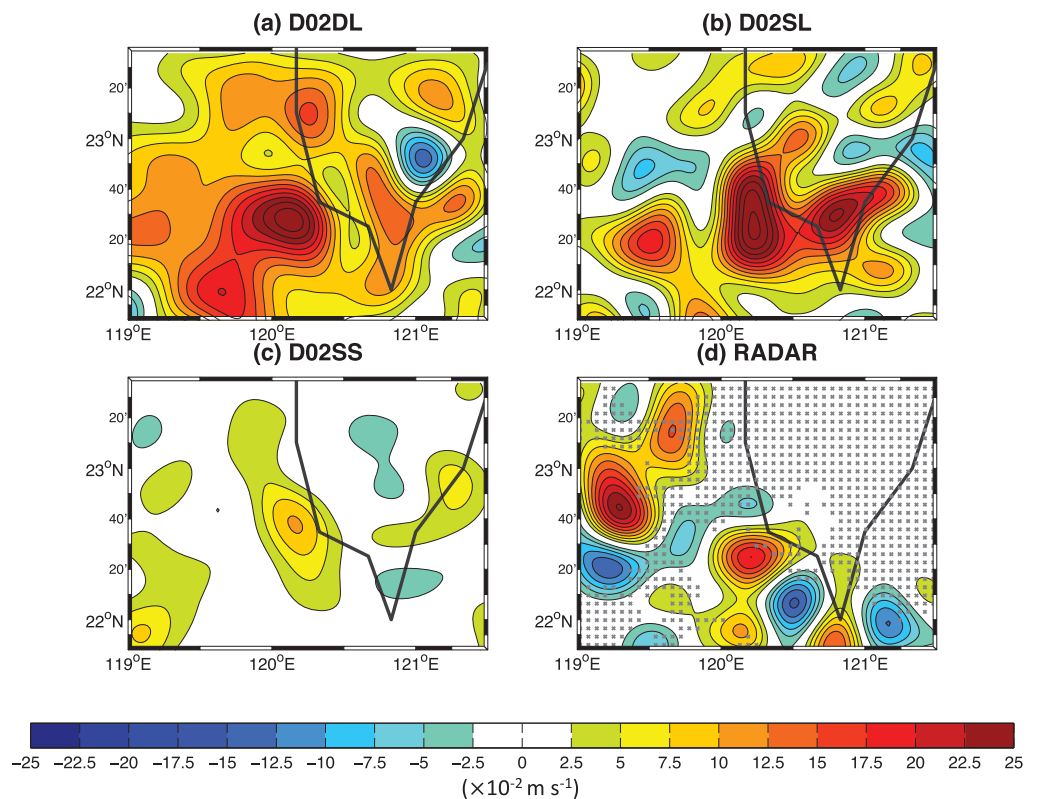


Figure 5. Vertical velocity (m s^{-1}) from (a) D02DL, (b) D02SL, and (c) D02SS analyses, and from (d) radar observation at 700 hPa at 1800 UTC 15 June. The radar data in Figure 5d is rescaled by a factor of 0.5.

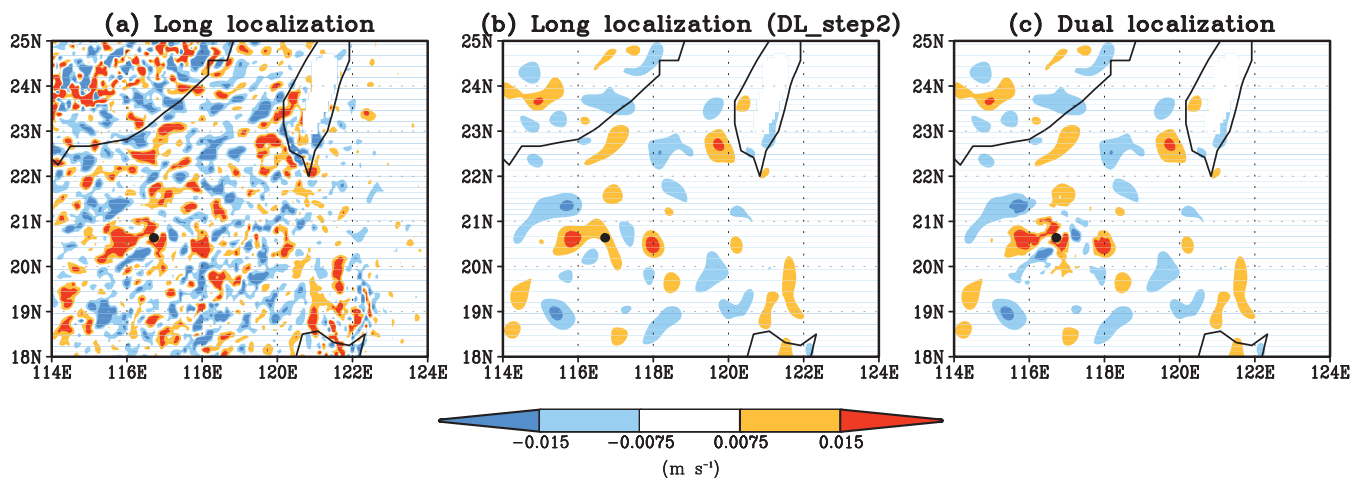


Figure 6. Vertical wind speed analysis increments (m s^{-1}) at 850 hPa from the assimilation of a radiosonde at Dongsha (116.7200°E , 20.6700°N ; black dots) at 1200 UTC 15 June 2008.

distances. With this observation, vertical velocity correction at and near the observation is positive below 800 hPa. The analysis corrections with a long localization (Figure 6a) result in strong upward motion corrections near Dongsha and display numerous small-scale features across a wide area from the South China Sea to the Taiwan strait, as well as the coastal areas of southwestern Taiwan, the location of interest for the heavy rainfall event. In other words, assimilating the Dongsha radiosonde with a long localization can affect small-scale vertical motion in Taiwan. Such increments may be unrealistic but are common when using a high-resolution background ensemble due to spurious error correlations caused by sampling errors. Using a short localization can help eliminate these small-scale corrections which can appear far from their source observation(s).

The result of the second step in the dual-localization process, which is created using only the small-wave number components of the ensemble perturbations and a long localization, produces large-scale corrections near the observation, in the prefrontal area along the southeast coast of China and offshore of southwestern Taiwan (Figure 6b). The differences between Figures 6a and 6b demonstrate again that the second step of the DL method removes the large-wave number components of ensemble perturbations to avoid producing unrealistic small-scale analysis corrections for synoptic-scale features. The final vertical wind analysis corrections from the DL method (Figure 6c) include not only local, mesoscale features near the observation location, but also synoptic-scale features over the frontal area from Figure 6b. Taken together, Figures 4b and 6c show that assimilating the Dongsha radiosonde using the DL method promotes significant horizontal moisture transport toward Taiwan, but avoids creating strong, small-scale vertical motions along the moisture transport pathway.

To summarize, our results demonstrate that the DL method can derive multiscale analysis corrections for a complex, multiscale weather system—such as the Meiyu rainfall event described here—without having to make any arbitrary adjustments. These qualities are important for producing accurate forecasts of long-duration heavy rainfall events. The D02SS and D02SL analysis corrections, on the other hand, which were produced using a single short and a single long localization, respectively, failed to produce sufficient synoptic-scale moisture transport and were characterized by unrealistic, widespread small-scale convergence/vertical motion, respectively. The benefit of the DL method (i.e., D02DL) is demonstrated further in the next section with an evaluation of the rainfall forecasts for the three experiments.

4. Forecast Results

We begin the forecast evaluation by examining the first 6 h accumulated rainfall over the South China Sea to provide an example of deficiencies that may arise in open-ocean rainfall forecasts when using a single long localization in high-resolution analysis corrections. Note that for all experiments, forecasts are initialized by the ensemble analysis means at 1200 UTC, 15 June. During the first 6 h of the forecast period, heavy

rainfall was observed over the South China Sea in CMORPH data (Figure 7a), indicating the presence of active mesoscale convective systems in the region. Of the three experiments, D02DL (Figure 7b) is the only one whose forecast produces a mesoscale convective system and an associated area of heavy rainfall over the South China Sea (near 21°N), even though it too fails to reproduce the large area of convection and rainfall further south. While it is not surprising that D02SS misses this rainfall (Figure 7d) since it is much drier over the South China Sea than the other experiments, it is surprising that D02SL (Figure 7c) misses it as well despite having higher synoptic-scale moisture levels over the region than D02SS. This is partially due to overactive small-scale features which may have interfered with the development of mesoscale convective systems during the data cycling period.

It is notable that both D02DL and D02SL produce heavy rainfall over southwestern Taiwan during the first 6 h of the forecast period even though no such heavy rainfall was observed (Figure 7). Initializing the forecasts at 1800 UTC, 15 June avoids this problem but ultimately has little effect on the forecast period thereafter. Thus, we will continue to examine only the results of the forecasts initialized at 1200 UTC, 15 June. The

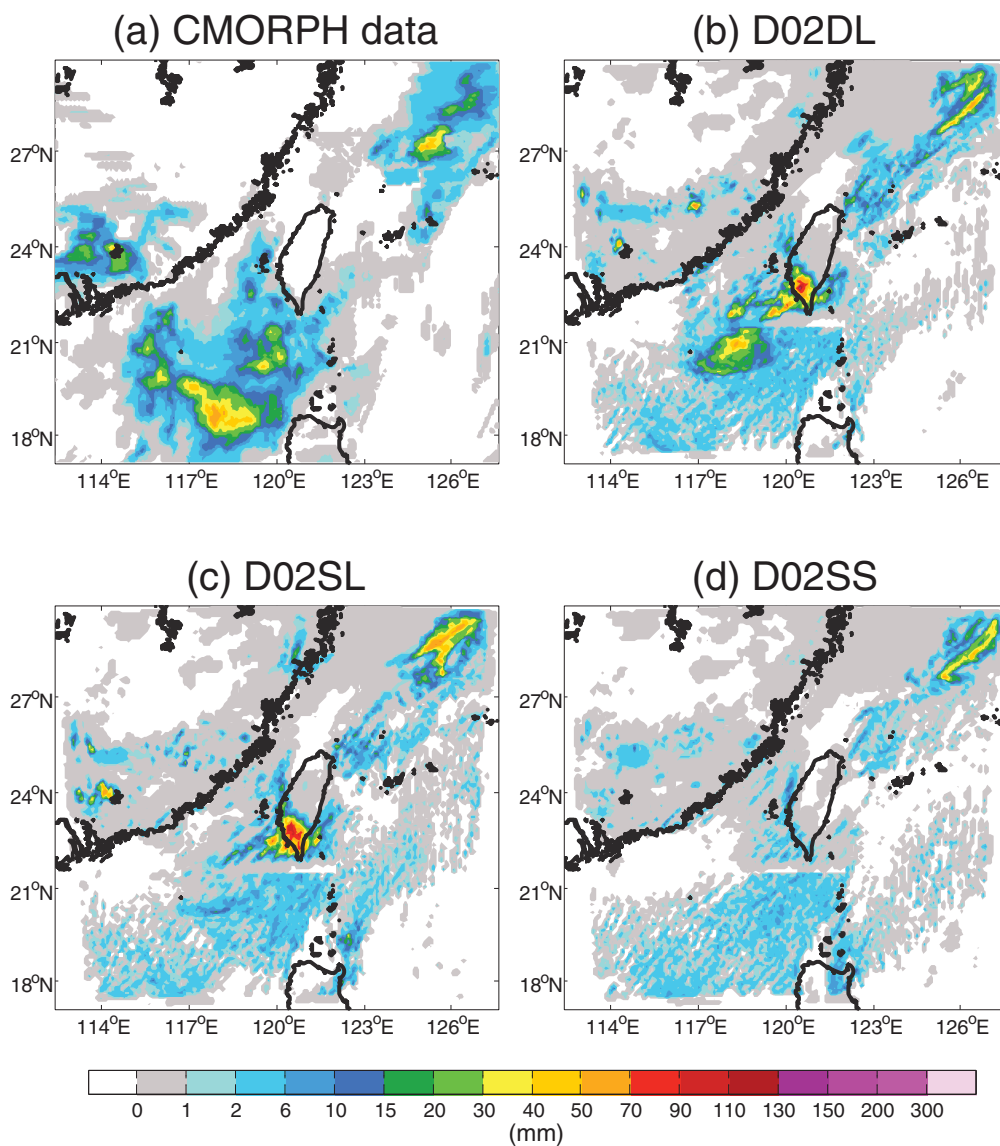


Figure 7. Six hour accumulated rainfall (mm), from 1200 UTC to 1800 UTC 15 June 2008 from the (a) CMORPH data (satellite-derived precipitation product) and (b) D02DL, (c) D02SL, and (d) D02SS.

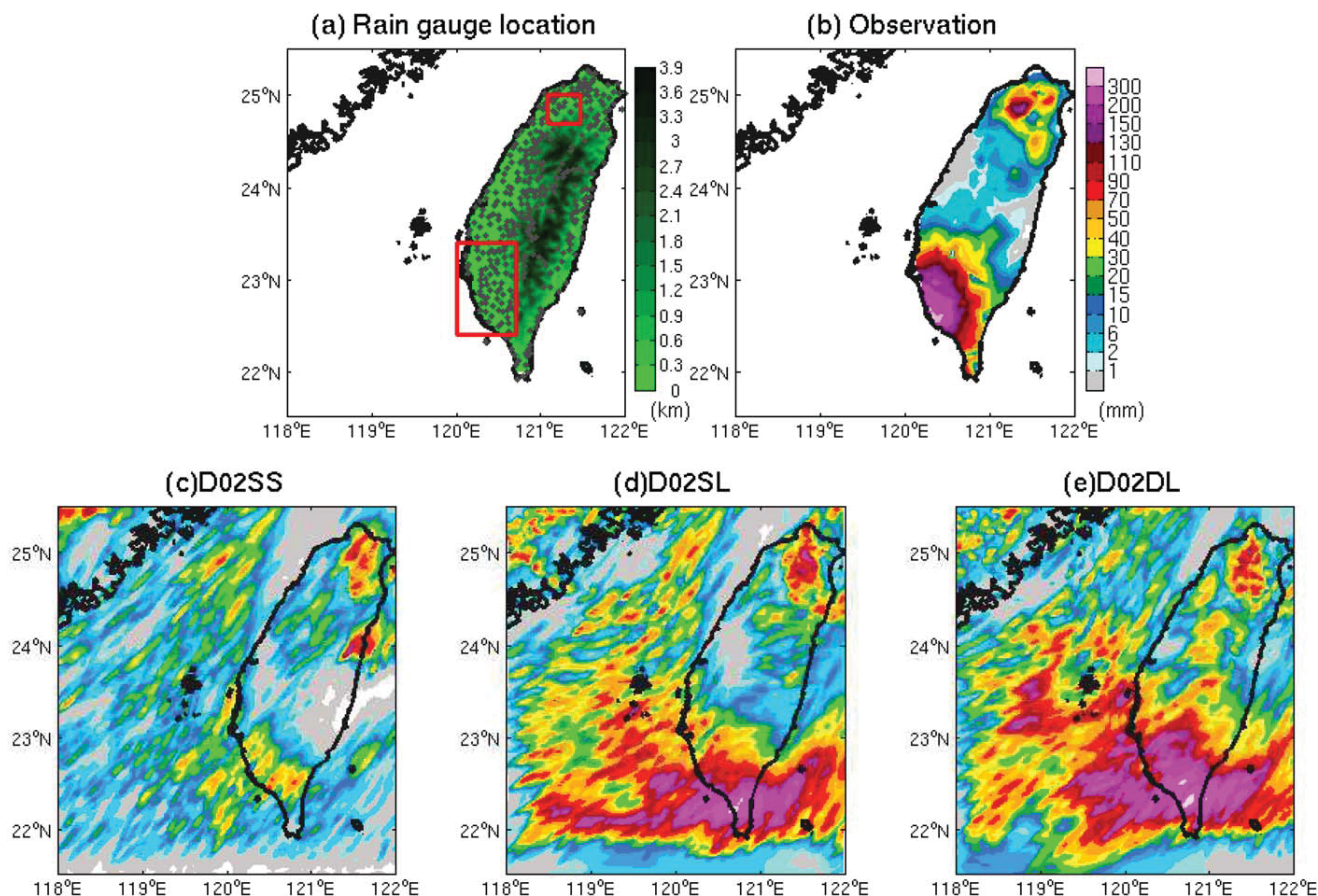


Figure 8. (a) Rain gauge locations and the topography in Taiwan. Daily rainfall accumulation (mm), from 0000 LST 16 June 2008 to 0000 LST 17 June 2008, from (b) rain gauge observations, (c) D02SS, (d) D02SL, and (e) D02DL. The large and small red boxes in Figure 8a indicate the averaging areas used to produce Figures 9a and 9b, respectively.

following discussion examines and compares the characteristics of the accumulated rainfall on 16 June for the three experiments, focusing on two geophysical areas: southwestern and northern Taiwan (Figures 8a and 8b). Heavy rainfall in the former covered a larger area and was more prolonged (~20 h versus ~8 h) than in the latter.

4.1. Evaluation of the Spatial Distribution of Heavy Rainfall

Figures 8c–8e show the forecasted 24 h accumulated rainfall on 16 June for domain-3. The single short localization experiment (D02SS) significantly underestimates the 24 h accumulated rainfall between 1600 UTC, 15 June and 1600 UTC, 16 June (i.e., 0000 LST, 16 June to 0000 LST, 17 June local time) over southwestern Taiwan (Figure 8c). This is caused by the underestimation of the large-scale moisture transport toward Taiwan resulting from the absence of large-scale analysis corrections. On the other hand, both D02SL and

D02DL show heavy rainfall over southwestern Taiwan (Figures 8d and 8e) in better agreement with observations. Compared to D02SS, D02SL produces a much more skillful forecast (see Threat Scores (TS) for different thresholds of accumulated rainfall in Table 1). This can be attributed to the D02SL analysis having a better representation of the large-scale moisture transport and greater convergence just offshore of southwestern Taiwan. However, the heaviest rainfall in D02SL is located south of the

Table 1. The Threat Scores (TSs) of 24 h Accumulated Heavy Rainfall at Southwestern Taiwan^a

Experiment	80 mm	100 mm	130 mm	150 mm
D02DL	0.8750	0.8085	0.5581	0.3889
D02SL	0.3958	0.2667	0.0556	0.0000
D02SS	0.0000	0.0000	0.0000	0.0000

^aThe rainfall is accumulated from 1600 UTC 15 (0000 LST 16) June to 1600 UTC 16 (0000 LST 17) June from experiments initialized at 1200 UTC 15 June 2008. The coverage area to calculate the scores is indicated in Figure 8a.

observed precipitation maximum, causing the forecasted rainfall amount in southwestern Taiwan to be much less than observed.

Compared to the D02SL forecast, that of D02DL shows higher rainfall amounts over a larger area of southwestern Taiwan (Figure 8d versus Figure 8e). This is mainly due to higher moisture levels in the upstream environment stemming from the analysis moisture corrections as well as stronger low-level southerly flow along the coast of southwestern Taiwan (figure not shown). Of the two experiments, D02DL better predicts the distribution of heavy rainfall, leading to higher Threat Scores (TSs) for the heavy rainfall on 16 June (Table 1). The use of a single long localization in domain-2 analysis of D02SL causes the resulting forecast to not only miss the heavy rainfall over the South China Sea during the first 6 h, as discussed earlier, but also misplace the area of maximum rainfall in southwestern Taiwan on 16 June.

In addition to the heavy rainfall over southwestern Taiwan, the forecasts for both D02DL and D02SL (Figures 8d and 8e) also capture the small-area of brief but very intense rainfall in northern Taiwan (the mountainous region near Taoyuan City). However, its forecasted location in D02SL is shifted slightly eastward of its observed location due to stronger forecasted westerly winds. The D02SS forecast accurately captures the location of this rainfall (Figure 8c) but greatly underestimates its intensity.

Since the forecasted rainfall over both southwestern and northern Taiwan in D02SS is much worse than that in D02SL and D02DL, the discussion below will focus primarily on the comparison between D02SL and D02DL.

4.2. Evaluation of the Time Evolution of Heavy Rainfall

Correctly predicting flash flooding depends on the accuracy of very short-term rainfall forecasts rather than forecasts of daily rainfall accumulations. Thus, we now evaluate the experiments on their ability to correctly reproduce the temporal evolution of rainfall by comparing forecasted and rain gauge-observed average hourly rainfall rates over southwestern and northern Taiwan (Figure 9). It cannot be overemphasized that the high-intensity, small-scale, short-term rainfall responsible for severe flash flooding is very difficult to predict.

Within a span of 20 h, observations show four peaks in the rainfall intensity over southwestern Taiwan (Figure 9a). Forecasted rainfall in southwestern Taiwan for both D02DL and D02SL occurs earlier than observed and is highly overpredicted, consistent with the previously discussed false heavy rainfall that occurred in the region during the first 6 h of the forecast period. This false rainfall signature could have been eliminated and the first rainfall peak better simulated, particularly for D02DL, if the forecasts were initialized by the ensemble analysis mean at

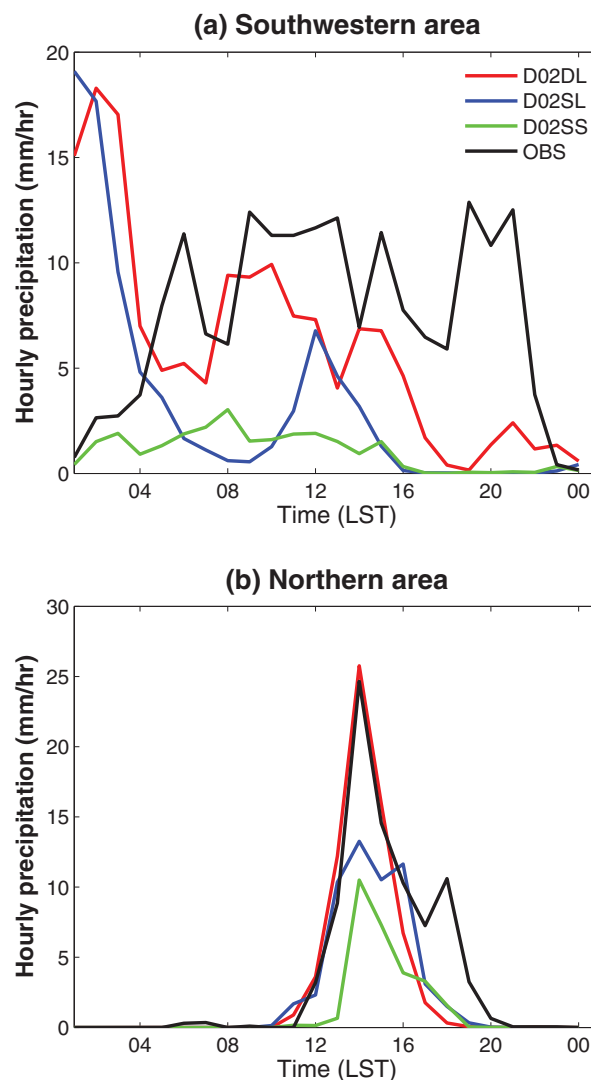


Figure 9. Time series of the hourly rainfall (mm/h) averaged over areas in (a) southwestern (the large red box in Figure 8a) and (b) northern (the small red box in Figure 8a) Taiwan from observation and forecasts initialized at 1200 UTC 15 June 2008.

1800 UTC rather than 1200 UTC, 15 June. This is partially due to the availability of radiosonde observations over the rainfall area in the southwestern Taiwan at 1800 UTC, which produced local analysis corrections at that time that ultimately helped to improve rainfall prediction over the region. Nevertheless, while both D02DL and D02SL fail to capture the first observed rainfall peak, D02DL better predicts the magnitude, timing, and duration of the second and third peaks. D02SS, on the other hand, misses all four rainfall peaks.

The forecasted temporal evolution of the heavy rainfall event in northern Taiwan differs significantly for each experiment (Figure 9b). The D02DL forecast perfectly captures the timing and intensity of the first, main rainfall peak, but brings rainfall to an end earlier than observed. The D02SL forecast also accurately captures the timing of the main rainfall peak but underestimates its intensity in the region of interest due to an eastward shift in the simulated precipitation maximum. It also terminates the rainfall event prematurely, similar to D02DL. In the D02SS forecast, the rainfall event is delayed and, as expected, its peak intensity is the weakest of the three experiments.

We conclude that the rainfall forecasts for northern Taiwan further support the idea that both large- and small-scale analysis corrections can be critical for accurately predicting the location, timing, and intensity of brief heavy rainfall events.

To quantitatively demonstrate the benefit of the D02DL forecast in simulating the time evolution of rainfall intensity, the Rank Probability Score (RPS), which considers a multievent forecast situation, is computed for each forecast and compared [Wilks, 2005]. Note that only the forecasts for the heavy rainfall event in southwestern Taiwan is examined as there are too few rain gauges in the area of the northern rainfall event for a proper statistical evaluation. The RPS measures the squared-error score with respect to an observation value of "1" if the forecast event occurs, and "0" if it does not occur. In order for the score to be sensitive to the probabilities of a multievent situation, the RPS is computed with respect to the cumulative probabilities in the forecast and observation, such as events with forecast rainfall rates falling within the following ranges: <1, 1–5, 5–10, and >10 mm/h, from light to intense rainfall. More accurate forecasts have smaller RPS values. Figure 10a shows the RPS time series for the D02SS, D02SL, and D02DL forecasts, while Figure 10b shows the fraction of observation stations used in the RPS calculation reporting rainfall rates in each of the four rainfall "bins." With the exception of the first three hours, D02DL forecast has the lowest RPS score for much of the time series, indicating that it had the highest probability of predicting a rainfall

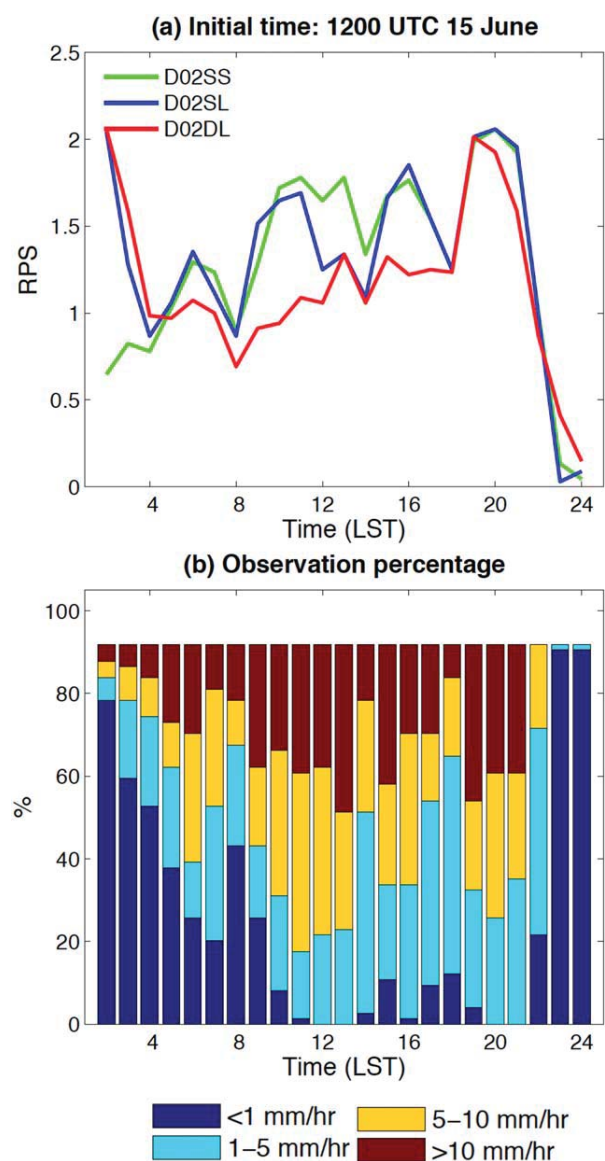


Figure 10. Time series of (a) the rank probability score for the rainfall forecasts over southwestern Taiwan (the large red box in Figure 8a), starting from 0000 LST 16 June 2008 and (b) the percentage of observation stations reporting rainfall rates within each range (<1, 1–5, 5–10, and >10 mm/h). There are 74 observation stations in the area of verification.

rate falling within the same range as an observed value at a given rain gauge site, especially during the rainfall intensity peaks. The average score is about 1.25 for both D02SL and D02SS and 1.08 for D02DL after the first 3 h of the forecast, further demonstrating the benefit of the D02DL forecast.

4.3. Radar Reflectivity

In addition to rainfall rates and accumulations, the forecasted mesoscale convective systems are evaluated through comparisons with radar observations. Figure 11 shows the observed and modeled composite radar reflectivities at 0800 and 1500 LST, 16 June (0000 UTC and 0700 UTC, 16 June, respectively). At 0800 LST, the observed radar image (Figure 11a) shows an area of strong convective rainband offshore of southwestern, southern, and southeastern Taiwan, as well as along the coastline of southwestern Taiwan. D02DL's forecasted reflectivity at this time captures the active convection over coastal areas of southwestern Taiwan as well as that offshore of Taiwan's southeast coast, but fails to reproduce most of the offshore convection to the south and southwest (Figure 11b), suggesting that the strong convection offshore of southwestern Taiwan moved inland earlier than observed. By comparison, the D02SL forecast shows relatively weak convection offshore of and over southwestern Taiwan (Figure 11c), while that of D02SS has only very limited convection in that area (Figure 11d).

At 1500 LST, strong radar reflectivities were observed over a large area over and to the southwest of southwestern Taiwan (Figure 11e), marking an extended period of heavy rainfall over the region. Although both D02SL and D02DL fail to capture the full extent of the heavy rainfall southwest of Taiwan at this time, convection in the area is much stronger and more widespread in the D02DL forecast (Figure 11f versus Figure 11g), showing why heavy rainfall in southwestern Taiwan was more persistent in D02DL than D02SL. Nevertheless, the lack of convection offshore in Figures 11f and 11g also partially explains why the forecasted heavy rainfall event in southwestern Taiwan ends earlier than observed for both experiments (Figure 9a). This in turn is due to inadequate moisture transport from the South China Sea. It is also notable that the

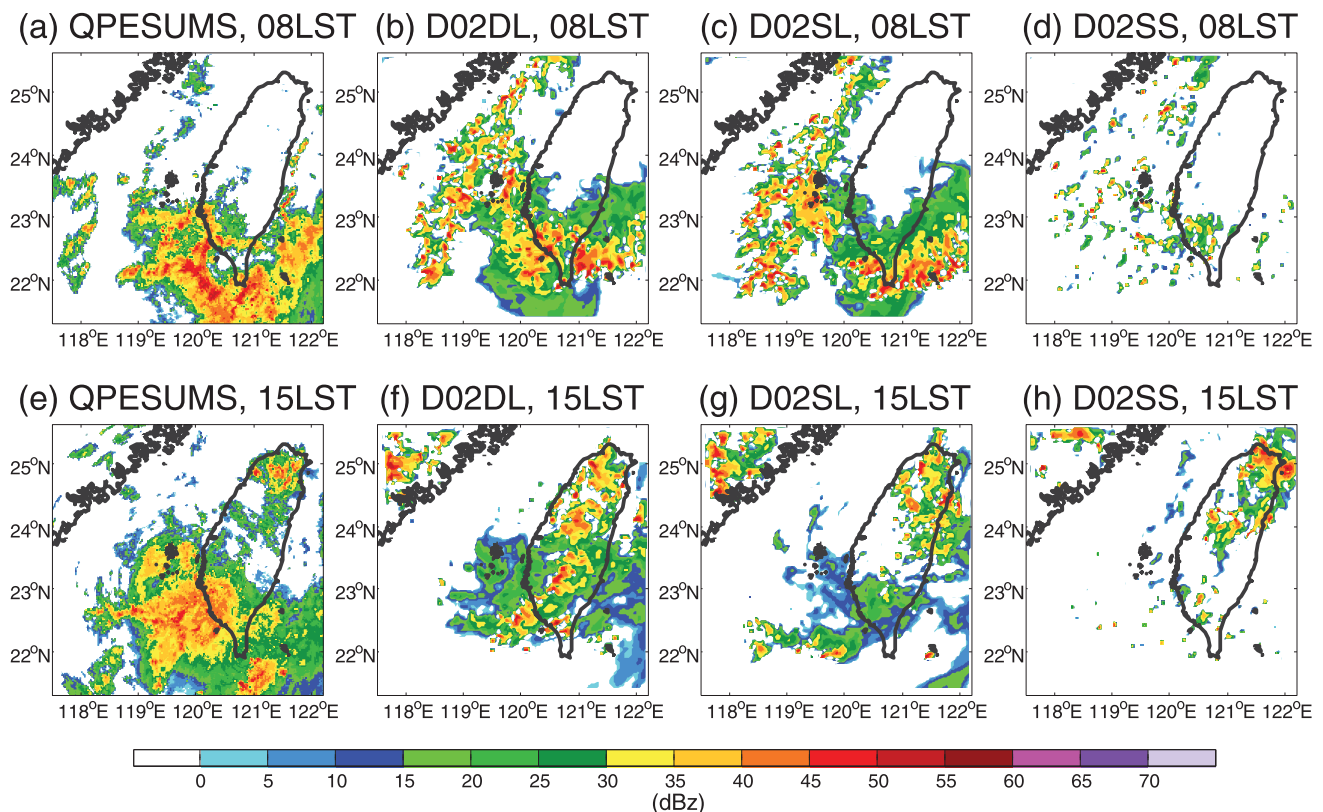


Figure 11. Composite radar reflectivity (dBz) at 0800 LST (0000 UTC) 16 June 2008 from (a) observations and (b) D02DL, (c) D02SL, and (d) D02SS after 12 h forecast. Figures 11e–11h are the same as Figures 11a–11d, respectively, except at 1500 LST (0700 UTC) 16 June (19 h forecast). Observations are taken from the quantitative precipitation estimation and segregation using multiple sensors (QPESUMS).

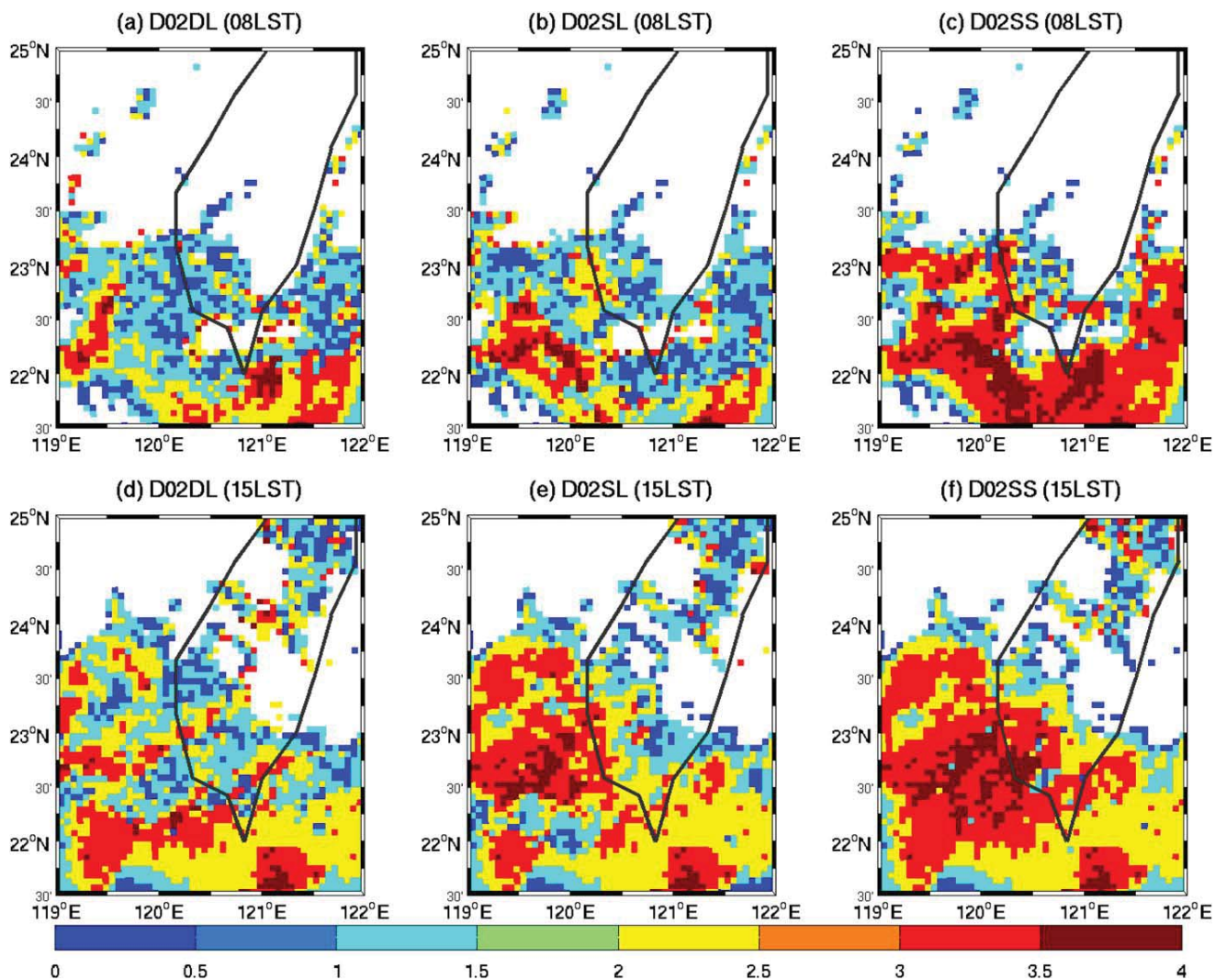


Figure 12. Map of rank probability score of the forecasted composite reflectivity against radar observations from (a) D02DL, (b) D02SL, and (c) D02SS at 0800 LST (0000 UTC) on 16 June 2008. Figures 12d–12f are the same as Figures 12a–12c, respectively, except at 1500 LST (0700 UTC) on 16 June 2008. Data in Figure 11 are used for calculation.

forecasts for both D02DL and D02SL call for heavy rainfall in southern Taiwan as well even though no such heavy rainfall was seen in the rain gauge observations. We suspect that this may be due to the underestimation of observed rainfall in the region caused by sparse rain gauge coverage (see dots in Figure 8a).

Our qualitative comparison of composite radar reflectivities can be given a quantitative foundation through the use of the RPS. Figure 12 shows the RPS values calculated at each model grid point using the following reflectivity ranges: <10, 10–20, 20–30 and 30–40, >40 dBZ. Here, emphasis is placed on the forecasts' ability to correctly reproduce observed spatial patterns of convection across a large portion of the domain. At 0800 LST, the RPS of the D02DL is much smaller (i.e., better) than those of D02SL and D02SS, particularly over the area extending from the South China Sea to Taiwan's southwestern coast. The D02DL forecast remains the superior option at 1500 LST (Figure 12d), again most notably along and offshore of Taiwan's southwestern coast. The superior skill of the D02DL forecast at both times is attributed to a better representation of the location and extent of mesoscale convective systems.

4.4. Ensemble Forecasts

In addition to the deterministic forecasts initialized from analysis means, the ability of each experiment to forecast the heavy rainfall event in question is evaluated in terms of its probabilistic quantitative

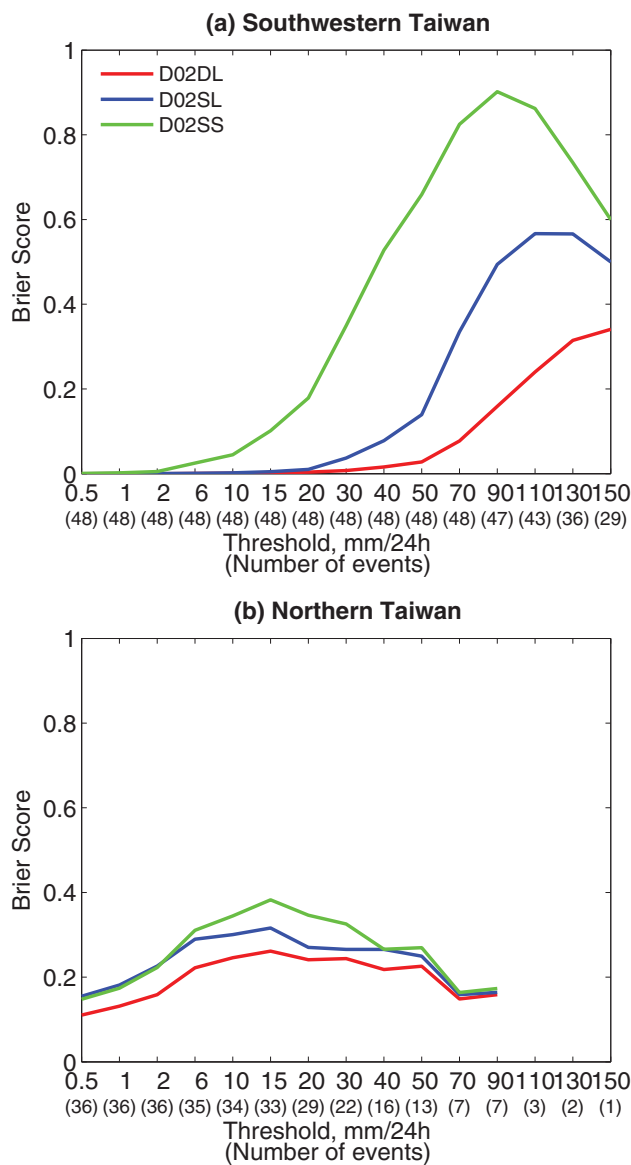


Figure 13. The Brier score of the 24 h, from 0000 LST 16 June to 0000 LST 17 June, probability quantitative precipitation forecast for the (a) southwestern (120.2°E–120.7°E, 22.4°N–23.2°N) and (b) northern Taiwan (121.0°E–121.8°E, 24.75°N–25.05°N). The area used in Figure 13a is the same as the lower red box indicated in Figure 8a, but the area used in Figure 13b is larger to have enough observations for calculation. Note that BS is calculated only when the number of events is larger than 5.

precipitation forecast (PQPF) derived from the ensemble forecasts. The PQPF in this study is verified by the Brier score (BS). The BS represents the mean squared error of the PQPF, where an observation is assigned a value of one if a specific event occurs and zero if it does not. Since the forecast and observation values lie between zero and one, the BS must also fall somewhere within the same range. A higher BS score indicates a less skillful forecast and BS = 0 indicates a perfect forecast.

Figure 13a shows each experiment's BS across a range of 24 h accumulated PQPF thresholds in southwestern and northern Taiwan. D02DL clearly has the smallest BS for all thresholds in southwestern Taiwan, especially for high rainfall accumulations (>50 mm/24 h). The D02SS ensemble forecasts consistently display the poorest skill, while the skill of the D02SL forecasts falls between those of D02DL and D02SS. The higher scores of the D02SL PQPF in southwestern Taiwan, relative to those of the D02DL PQPF, are again due to the shift of D02SL's forecasted precipitation maximum south of its observed location. Similarly, D02DL also produces the best 24 h PQPF in northern Taiwan (Figure 13b). Thus, the probabilistic ensemble precipitation forecasts support the conclusion of the deterministic forecasts that the DL method produces a superior forecast product for this case, improving not only the analysis corrections for the mean state but also the characteristics of the ensemble perturbations such that they better represent the uncertainties related to this heavy rainfall event.

5. Conclusions

The regional WRF-LETKF analysis system developed at National Central University (NCU) has been extended to allow multiscale, multiresolution assimilation using the dual-localization (DL) method introduced by Miyoshi and Kondo [2013]. The extended system is used to study a heavy rainfall event associated with a Meiyu front that passed through Taiwan on 16 June 2008. The Meiyu front in this case is a typical example of a multiscale weather system, as it involves interactions between large-scale southwesterly monsoonal flow over the South China Sea, a mesoscale front, one or more mesoscale convective systems, and storm-scale convective cells, all of which may additionally interact with complex terrain.

One reason for assimilating observations on a high-resolution nested domain is to obtain small-scale analysis corrections. For high-resolution EnKF assimilation, a small covariance localization is commonly used to avoid sampling errors that may occur over longer distances. However, such an approach can eliminate critical large-scale corrections appearing in the analysis. In this case, such corrections included those affecting large-scale moisture transport from the ocean toward Taiwan, which proved essential for producing accurate Meiyu rainfall forecasts. The use of the DL method for assimilation on a high-resolution inner-domain permits both large and small-scale analysis corrections to appear simultaneously.

Three numerical experiments—D02SS, D02SL, and D02DL—are conducted. For each experiment, two-domain data assimilation, beginning at 0000 UTC, 15 June 2008, is followed by a three-domain forecast initialized at 1200 UTC, 15 June. The experiments differ only in the localization strategy used for assimilation on the inner domain. D02SS and D02SL use single localizations of 60 and 360 km, respectively, while D02DL uses the dual-localization method. Rainfall forecasts over southwestern and northern Taiwan on 16 June for all experiments were compared against observations and each other to evaluate the impact of the DL method.

The use of a long localization (i.e., D02SL and D02DL) produces large-scale corrections affecting the moisture transport from the ocean toward Taiwan via southwesterly monsoonal flow over the South China Sea. These corrections play a critical role in sustaining the moisture supply needed to produce reasonable rainfall forecasts for southwestern Taiwan. However, unlike the analysis of D02DL, that of D02SL contains an extensive area of unrealistic small-scale features over the South China Sea, caused by the application of the long localization to the full resolution ensemble perturbations. D02DL avoids this issue by applying the long localization only to the small wave number components of the ensemble perturbations.

The use of a single short localization (e.g., D02SS), on the other hand, helps correct small-scale features near the observation locations, including the magnitude of convergence and vertical motions in near-coastal areas of southwestern, southern, and northern Taiwan, but does not include any large-scale corrections. By combining both large- and small-scale corrections in a methodical, nonarbitrary way, the D02DL analysis provides the initial conditions best suited for triggering and sustaining strong convection in the forecast.

The spatial and temporal characteristics of the rainfall forecasts initialized at 1200 UTC 15 June from the three experiments on 16 June 2008 were evaluated against rain gauge, radar, and satellite-derived precipitation observations. Without corrections to the large-scale moisture transport, D02SS significantly underpredicted rainfall over southwestern Taiwan. On the other hand, the D02SL and D02DL forecasts, initialized with analyses that included large-scale corrections, successfully captured the rainfall event over the area, but nevertheless had trouble reproducing the timing and magnitude of first observed peak in the rainfall intensity. All things considered, however, the D02DL rainfall forecast for southwestern Taiwan proved to be the better option, particularly since the rainfall maximum in the D02SL forecast was shifted south of its observed location. Additionally, the D02DL forecast better captured the observed temporal evolution of the rainfall intensity as well as the overall duration of the heavy rainfall event. Despite also benefitting from large-scale analysis corrections, the D02SL rainfall forecast is degraded by the presence of unrealistically extensive small-scale features which interfered with large-scale moisture transport from the South China Sea. A quantitative assessment of the forecasts using Threat Scores and Rank Probability Scores confirmed the benefit of the D02DL forecast for both the rainfall distribution and total area-averaged accumulations. D02DL also produced the highest forecast skill for the prediction of the short-lived but intense period of heavy rainfall over northern Taiwan. Finally, Brier scores for each experiment's probabilistic quantitative precipitation forecasts for southwestern and northern Taiwan across a range of different rainfall thresholds showed that the use of the DL method (i.e., D02DL) improves not only the deterministic forecast initialized with the ensemble analysis mean, but also the ensemble forecasts.

All the advantages from the D02DL analyses/forecasts in this study demonstrate the importance of including multiscale analysis corrections when applying data assimilation to a high-resolution grid, particularly when forecasting weather systems dominated by multiscale interactions. Although this study only demonstrates the benefit of multilocalization, multiresolution data assimilation for a Meiyu-front precipitation case, the assimilation framework described and used here is expected to prove useful for improving forecasts for severe weather events characterized by multiscale interactions, including tropical cyclones [e.g., Huang and Lin, 2014]. Additional case studies will be conducted in the future to fully assess the advantages of the DL method in a variety of different scenarios.

Acknowledgments

Shu-Chih Yang is sponsored by the National Space Organization grant NSPO-S-105083 and the Ministry of Science and Technology grant MOST-105-2111-M-008-023. Shu-Hua Chen is partially supported by the U.S. National Science Foundation Award 1015910. Several data sets are used in this study, including field campaign data from the SoWMEX/TiMREX website (<http://p3rd.as.ntu.edu.tw/2008/index.php>), FNL data available at the Computational and Information Systems Laboratory at the National Center for Atmospheric Research, satellite wind from <http://tropic.ssec.wisc.edu/archive>, conventional meteorology observations and composite radar reflectivity from the Central Weather Bureau in Taiwan, and GPS RO data from NSPO-Taiwan Analysis Center for COSMIC. The authors thank Kenneth Earl for his proofread and comments on the manuscript and Cheng-Chieh Kao for technical support.

References

- Davis, C. A., and W.-C. Lee (2012), Mesoscale analysis of heavy rainfall episodes from SoWMEX/TiMREX, *J. Atmos. Sci.*, *69*, 512–537.
- Dudhia, J. (1989), Numerical study of convection observed during the winter monsoon experiment using a mesoscale two dimensional model, *J. Atmos. Sci.*, *46*, 3077–3107.
- Grell, G. A., and D. Dévényi (2002), A generalized approach to parameterizing convection combining ensemble and data assimilation techniques, *Geophys. Res. Lett.*, *29*(14), doi:10.1029/2002GL015311.
- Greybush, S., E. Kalnay, T. Miyoshi, K. Ide, and B. R. Hunt (2012), Balance and ensemble Kalman Filter localization techniques, *Mon. Weather Rev.*, *139*, 511–522.
- Hong, S.-Y., Y. Noh, and J. Dudhia (2006), A new vertical diffusion package with an explicit treatment of entrainment processes, *Mon. Weather Rev.*, *134*, 2318–2341, doi:10.1175/MWR3199.1.
- Houtekamer, P., and F. Zhang (2016), Review of the ensemble kalman filter for atmospheric data assimilation, *Mon. Wea. Rev.*, *144*, 4489–4532.
- Houtekamer, P. L., and H. L. Mitchell (1998), Data assimilation using an ensemble Kalman filter technique, *Mon. Weather Rev.*, *126*, 796–811.
- Huang, Y.-C., and Y.-L. Lin (2014), A study on the structure and precipitation of Morakot (2009) induced by the Central Mountain Range of Taiwan, *Meteorol. Atmos. Phys.*, *123*, 115–141.
- Hunt, H. R., E. J. Kostelich, and I. Szunyogh (2007), Efficient data assimilation for spatiotemporal chaos: A local ensemble transform Kalman filter, *Physica D*, *230*, 112–126.
- Jou, B. J.-D., W.-C. Lee, and R. H. Johnson (2011), An overview of SoWMEX/TiMREX and its operation, in *The Global Monsoon System: Research and Forecast*, 2nd ed., edited by C.-P. Chang et al., pp. 303–318, World Sci.
- Kondo, K., T. Miyoshi, and H. L. Tanaka (2013), Parameter sensitivities of the dual-localization approach in the local ensemble transform Kalman filter, *SOLA*, *9*, 174–177, doi:10.2151/sola.2013-039.
- Li, Z., J. C. McWilliams, K. Ide, and J. Farrara (2015), A multiscale variational data assimilation scheme: Formulation and illustration, *Mon. Weather Rev.*, *143*, 3804–3822.
- Liou, Y.-C., S.-F. Chang, and J. Sun (2012), An application of the immersed boundary method for recovering the three-dimensional wind fields over complex terrain using multiple-Doppler radar data, *Mon. Weather Rev.*, *140*, 1603–1619.
- Liou, Y.-C., J.-L. Chiu, W.-H. Chen, and H.-Y. Yu (2014), Improving the model convective storm quantitative precipitation nowcasting by assimilating state variables retrieved from multiple-Doppler radar observations, *Mon. Weather Rev.*, *142*, 4017–4035.
- Miyoshi, T., and K. Kondo (2013), A multi-scale localization approach to an ensemble Kalman filter, *SOLA*, *9*, 170–173, doi:10.2151/sola.2013-038.
- Miyoshi, T., K. Kondo, and T. Imamura (2014), The 10,240-member ensemble Kalman filtering with an intermediate AGCM, *Geophys. Res. Lett.*, *41*, 5264–5271, doi:10.1002/2014GL060863.
- Mlawer, E. J., S. J. Taubman, P. D. Brown, M. J. Iacono, and S. A. Clough (1997), Radiative transfer for inhomogeneous atmosphere: RRTM, a validated correlated-k model for the longwave, *J. Geophys. Res.*, *102*, 16 663–16 682, doi:10.1029/97JD00237.
- Poterjoy, J., F. Zhang, and Y. Weng (2014), The effects of sampling errors on the EnKF assimilation of inner core hurricane observations, *Mon. Weather Rev.*, *142*, 1609–1630.
- Pu, Z., S. Zhang, M. Tong, and V. Tallapragada (2016), Influence of the self-consistent regional ensemble background error covariance on hurricane inner-core data assimilation with the GSI-based hybrid system for HWRF, *J. Atmos. Sci.*, *73*, 4911–4925.
- Raynaud, L., L. Berre, and G. Desroziers (2009), Objective filtering of ensemble-based background error-variances, *Q. J. R. Meteorol. Soc.*, *135*, 1177–1199.
- Skamarock, W. C. (2004), Evaluating Mesoscale NWP Models Using Kinetic Energy Spectra, *Mon. Wea. Rev.*, *132*, 3019–3032.
- Skamarock, W. C., and J. B. Klemp (2008), A time-split nonhydrostatic atmospheric model for weather research and forecasting applications, *J. Comput. Phys.*, *227*, 3465–3485, doi:10.1016/j.jcp.2007.01.037.
- Sun, J., et al. (2014), Use of NWP for nowcasting convective precipitation: Recent progress and challenges, *Bull. Am. Meteorol. Soc.*, *95*, 409–426.
- Tao, W.-K., D. Baker, J. Simpson, and P. Wetzel (2003), Microphysics, radiation and surface processes in the Goddard Cumulus Ensemble (GCE) model, *Meteorol. Atmos. Phys.*, *82*, 97–137, doi:10.1007/s00703-001-0594-7.
- Tsai, C.-C., S.-C. Yang, and Y.-C. Liou (2014), Improving short-term QPFs with a WRF-LETKF radar data assimilation system: OSSEs on Typhoon Morakot (2009), *Tellus, Ser. A*, *66*, 21804.
- Tu, C.-C., Y.-L. Chen, C.-S. Chen, P.-L. Lin, and P.-H. Lin (2014), A comparison of two heavy rainfall events during the Terrain-Influenced Monsoon Rainfall Experiment (TiMREX) 2008, *Mon. Weather Rev.*, *142*, 2436–2463.
- Tu, C.-C., Y.-L. Chen, S.-Y. Chen, Y.-H. Kuo, and P.-L. Lin (2017), Impacts of including rain- evaporative cooling in the initial conditions on the prediction of a coastal heavy rainfall event during TiMREX, *Mon. Weather Rev.*, *145*, 253–277.
- Wilks, D. S. (2005), *Statistical methods in the Atmospheric Sciences*, 2nd edition, pp. 648, Academic Press, Cambridge, Md.
- Whitaker, J. S., T. M. Hamill, X. Wei, Y. Song, and Z. Toth (2008), Ensemble data assimilation with the NCEP Global Forecast System, *Mon. Weather Rev.*, *136*, 463–481.
- Xu, W., E. J. Zipser, Y.-L. Chen, C. Liu, Y.-C. Liou, W.-C. Lee, B. J.-D. Jou (2012), An orography-associated extreme rainfall event during TiMREX: Initiation, storm evolution, and maintenance, *Mon. Weather Rev.*, *120*, 2555–2574.
- Yang, S.-C., K.-J. Lin, T. Miyoshi, and E. Kalnay (2013), Improving the spin-up of regional EnKF for typhoon assimilation and forecasting with Typhoon Sinlaku (2008), *Tellus, Ser. A*, *65*, 25804.
- Yang, S.-C., S.-H. Chen, S.-Y. Chen, C.-Y. Huang, and C.-S. Chen (2014), Evaluating the impact of the COSMIC-RO bending angle data on predicting the heavy precipitation episode on 16 June 2008 during SoWMEX-IOP8, *Mon. Weather Rev.*, *142*, 4139–4163.
- Zhang, F., C. Snyder, and J. Sun (2004), Impacts of initial estimate and observation availability on convective-scale data assimilation with an ensemble Kalman filter, *Mon. Weather Rev.*, *132*, 1238–1253.
- Zhang, F., Z. Meng, and A. Aksoy (2006), Tests of an ensemble Kalman filter for mesoscale and regional-scale data assimilation. Part I: Perfect model experiments, *Mon. Weather Rev.*, *134*, 722–736.
- Zhang, F., Y. Weng, J. A. Sippel, Z. Meng, and C. H. Bishop (2009), Cloud-resolving hurricane initialization and prediction through assimilation of Doppler radar observations with an ensemble Kalman filter, *Mon. Weather Rev.*, *137*, 2105–2125.
- Zhao, Q., F. Zhang, T. Holt, C. H. Bishop, and Q. Xu (2013), Development and testing of a mesoscale and storm-scale ensemble data assimilation system at the Naval Research Laboratory, *Weather Forecast.*, *28*, 1322–1335.